WIS-91/40/July-PH

28 pgs

Ultrafast Secondary Emission X-ray Imaging Detectors: A possible application to TRD

A. Akkerman,[1] A. Breskin, R. Chechik,[2] V. Elkind,
A. Gibrekhterman and S. Majewski[3]

The Weizmann Institute of Science
76100 Rehovot, Israel

Abstract

Fast high accuracy, X-ray imaging at high photon flux can be achieved when coupling thin solid convertors to gaseous electron multipliers, operating at low gas pressures. Secondary electrons emitted from the convertor foil are multiplied in several successive amplification elements. The obvious advantages of solid X-ray convertors, as compared to gaseous conversion, are the production of parallax-free images and the fast (sub-nanosecond) response. These X-ray detectors have many potential applications in basic and applied research. Of particular interest is the possibility of an efficient and ultrafast high resolution imaging of Transition Radiation, with a reduced dE/dx background.

We present experimental results on the operation of Secondary Emission X-ray (SEX) detectors, their detection efficiency, localization and time resolution. The experimental work is accompanied by mathematical modelling and computer simulation of Transition Radiation Detectors based on CsI TR convertors.

Presented at the 5th Pisa Symposium on Advanced Detectors
Elba-Italy, May 26-31, 1991

To be published in Nuclear Instruments and Methods in Physics Research A

[1] Soreq Nuclear Research Center, Yavne 70600, Israel

[2] The Hettie H. Heinemann Research Fellow

[3] Present address: CEBAF, Newport News, VA, U.S.A.

Introduction

In many fields of basic and applied research there is an increasing demand for efficient and accurate X-ray detectors. Many of the applications require the operation of such devices at very high X-ray flux and often in the presence of high radiation background of other sources like gamma-rays or charged particles. The required detectors often have to combine several properties like good energy resolution, high localization accuracy, high efficiency and high rate capability.

Ultrafast X-ray imaging over a broad energy range is requested in applications where the time resolved information is required for correlation with other phenomena or for trigger purposes, as for example, in particle identification with Transition Radiation (TR) and Synchrotron Radiation, or in diagnostics of high-temperature plasma. In X-ray diffraction experiments with high intensity Synchrotron Radiation Sources, such as studies of complex protein molecules, and for medical and industrial radiography and safety control, where the scanning time is of prime importance, there is a need for large area fast detectors with good localization capability allowing the operation at high radiation flux. In many of these applications the energy resolution is not necessary.

Traditional X-ray imaging methods, consisting of gaseous wire chambers of various types[1], are slow (100 ns typical resolution) and usually suffer from parallax errors in localization due to the different absorption depths of X-ray photons in the detection volume[2,3]. Furthermore, such devices suffer from serious efficiency problems at high rates and from radiation damage. There have been many improvements in small-surface soft X-ray imaging devices, based on various other techniques, as reviewed for example, in ref. 4.

A very interesting and unconventional idea for soft X-ray detection by using thin convertor foils coupled to gaseous multipliers was introduced by Margarian[5] for applications to TRD. A package of thin gold (Au) foils was proposed for TR photon conversion. Secondary electrons emitted from Au would ionize the gas and be detected. A similar idea was proposed for industrial radiography[6] (several hundred keV). It consists of a combination of metal convertor (tantalum) and an imaging wire chamber, placed at a

very low grazing angle with respect to the incident beam. A detection efficiency of the order of 30% is predicted for 400 keV photons. Very good imaging quality is achieved but there is a strong limit on the X-ray flux and the time resolution is limited to about 100 ns. The yield of emitted secondary electrons per absorbed X-ray depends on its energy, and on the composition and thickness of the convertor foil. Complete Monte Carlo calculations, based on mathematical models, which take into account the various processes involved in secondary electron transport and emission, can predict the efficiency of various convertors[7,8]. They confirm for example that in the energy range of 0.1–5 MeV tantalum convertors are the optimal choice. The most efficient convertor for soft X-rays seems to be CsI. Quantum efficiencies above 15% for solid and "spongy" (low density) CsI photocathodes, are reported by Kowalski et al.[11] for X-rays in the energy range of 0.1–9 keV. We would like to emphasize that metal convertors irradiated with soft X-rays-to-energetic gamma rays emit energetic secondary electrons ($E_e > 50$ eV). On the other hand, CsI irradiated with soft-to-hard X-rays emits mostly low energy secondary electrons ($E_e < 50$eV).

Henke et al.[9] have measured the energy spectra of electrons produced in vacuum by X-ray conversion in foils of Au, Al, CsI and CuI. It was found that the major part of electrons leaving the foil have very low energies, below 10 eV. As discussed below, these slow secondary electrons, emerging from the convertor, play a major role in the photon localization process. An important observation is that the energy spectra of secondary electrons induced by X-ray photons over a wide range of energies (0.3–10 keV) do not depend on the X-ray photon energy[9]. The fraction of the number of secondary (slow) photoelectrons in the total number of electrons emitted from Al and Au under the impact of 1.5 keV X-rays is of the order of 80-85% and in the case of CsI it is larger than 99.5%[9]. The secondary to total electron yield ratio goes down to 40% for Al and Au at X-ray energies of 8 keV, as derived from Monte Carlo calculations of Akkerman et al.[8], incorporating the experimental results of Henke et al.[9]. The electron yields and energy spectra in the case of CsI are presently being calculated by us. Based on the data of Schwarz[10], the absolute yield of secondary electrons per single absorbed X-ray pho-

ton in the energy range up to 10 keV was estimated to be of the order of 17 electrons for CsI and one electron for Al or Au convertor. Due to their high quantum yield CsI X-ray convertors have been used by several groups in combination with MCP detectors[12,13]. Similar systems have been successfully used also for detection of UV-photons[14].

We propose to couple convertor foils to highly efficient multi-stage avalanche **electron multipliers** operating at low gas pressures[15-17] as shown in fig. 1. The high amplification factors ($> 10^7$) reached in these **electron multipliers**[18] allow for high detection efficiency even of single electrons. Their high rate capability is derived from reduced space charge effects, due to fast ion removal and to a low charge density in the electron avalanche. The latter also reduces aging effects. The fast amplification mechanism leads to a subnanosecond time resolution[19]. Single electrons can be localized within an accuracy of the order of 200 μm FWHM[19].

Detectors based on this technique have been recently developed for UV-photon imaging with photosensitive gases (TMAE)[20,21] and for specific ionization measurements by single electron counting[22,23]. We have also developed gaseous UV-photomultipliers based on a CsI photocathode coupled to the low-pressure multistage electron multiplier[15-17]. The photomultipliers have imaging capability over a large active surface. The life-time of the CsI photocathode due to UV photons and ions impact was studied in detail[17].

The same technique can be used for X-ray detection. Ultrafast X-ray imaging at high photon flux can indeed be achieved by coupling thin foil convertors to low-pressure gaseous secondary electron multipliers[24].

We report on some results recently obtained with these Secondary Electron X-ray (SEX) detectors, operated with CsI, Al and Au convertors at an energy range of 6-60 keV. Our Monte Carlo simulations indicate that this method may be efficiently applied to Transition Radiation imaging with excellent time and localization resolutions, providing an interesting competitive solution for ultrarelativistic particle identification at future LHC/SSC colliders.

2. The Secondary Emission Detector and its Performance

Fig. 1 shows the structure of our prototype detector. It consists of several 80 mm diameter electrodes mounted in a vacuum vessel. All electrode frames are made of G-10 epoxy resin. A thin window, made of 100 μm Kapton, was used. The photocathode is made of a thin layer (400–2000 Å) of CsI, vacuum deposited on 200 Å of Al. The substrate is 2.5 μm thick Mylar. The metallic substrate is important for providing the potential to this electrode. The electrons emitted from the photocathode are immediately amplified in a 3 mm wide parallel gap. The avalanche electrons are transferred directly, or through a transfer gap (not shown in fig. 1), and further amplified in a MWPC element. The MWPC is equipped with cathode delay-line readout. A detailed description of this element and the readout system is given elsewhere[20]. The data acquisition and analysis is done with a PC computer interfaced to CAMAC based on electronics (ADC's and TDC's).

The detector was operated with 10-40 Torr of Ethane (C_2H_6) or dimethylether (DME). Both gases provide high gain, up to 10^7 for single electrons, in a single parallel gap and in a double stage amplification structure. However, DME provides a more stable operation with fewer secondary avalanches. Fig. 2 shows the amplification curve of a single parallel gap with DME at 20 Torr, when operated with UV photons. The detector was tested with 6-60 keV X-rays. Fig. 3a shows the pulse height spectrum obtained from a 2000 Å thick CsI photocathode, bombarded with 8 keV X-rays. For comparison a single photoelectron spectrum, induced by a UV lamp, is shown in fig. 3b. One can notice the large yield of secondary electrons emitted by the X-ray photons.

Saturated gain operation could be obtained in the multistep parallel plate mode with both C_2H_6 and DME as shown in fig. 4. Stable operation was obtained with both gases.

The quantum efficiency (QE) of the CsI convertors in our gaseous multiplier, was measured with 6 and 8 keV X-rays. For this purpose we calibrated our X-ray sources with a SiLi detector of known geometry. The SEX detector, operated with CsI convertors of 480 Å and 2000 Å, and with normal incidence of the X-ray beam, yielded a QE of

the order of 90–95% for the absorbed fraction of X-rays in these CsI layers. This demonstrates the high efficiency of the device for detecting secondary electrons.

The X-ray absorption and hence the absolute detection efficiency in these thin convertors is very low, of a few percent (fig. 6 θ=0°). In order to increase the detection efficiency a thick CsI layer has to be used. However, the thickness is limited so as to allow the secondary electrons to escape. The optimal thickness of the CsI layer depends on the X-ray photon energy and on the particular geometry used (transmittive or reflective photocathode). For the present geometry and energy range it is of the order of 2000 Å, as follows from Henke et al.[9] who measured the secondary electron yield as function of the CsI thickness and found a saturation in the yield at about 2000 Å (fig. 15 in ref. 9). Higher conversion efficiencies can be reached by using several layers of CsI foils coupled to independent detectors. Another possibility is the use of a grazing incidence angle geometry (fig. 5) which provides a larger absorption length for X-rays without increasing the actual thickness, and therefore without hindering electron extraction.

Fig. 6 shows the calculated conversion efficiency of CsI as function of the incident photon energy and the incidence angle. One can see that at 6 keV the efficiency of a 2000 Å thick CsI layer is of the order of 6% at θ=0° (normal incidence) and 30% at θ=80° (a grazing angle of 10°).

Another great advantage of a tilted geometry is the improvement in localization resolution in the projected dimension by a factor of cosθ. As an example the localization resolution at θ=80° will be of the order of 35 μm (FWHM), given the known intrinsic single electron localization resolution of such detectors, of the order of 200 μm (FWHM)[18].

The localization properties of our prototype detector were investigated with Al, Au, Al/CsI and Au/CsI convertors. Collimated X-ray beams of 8 and 17.5 keV were used. The anode of the MWPC has wires running at 45° with respect to each of the orthogonal wire planes of the cathodes, which ensures equal resolution in both dimensions. Fig. 7 shows 1D and 2D localization spectra measured with 8 keV X-rays and a CsI convertor. We could clearly note a striking difference between the response of the detector to

the different convertor materials. Best results have been obtained with Al/CsI. The best localization so far, measured at 8 keV with the Al/CsI convertor yielded an intrinsic resolution better than 200 μm (FWHM) (fig. 7). The resolutions obtained with Al and Au convertors are of the order of 1.2 mm and 0.5 mm (FWHM), respectively, at 8 keV. A localization resolution of 280 μm (FWHM) was measured with CsI at 17.5 keV.

The reason for the difference in response to the different convertor materials is in the nature of the electron emission mechanism. The conversion of an X-ray is followed by the emission of a primary electron (photoelectron) within the convertor material. This energetic (keV) primary electron may escape into the gas volume or may induce, by a cascade of electron-electron and electron-phonon interactions, low-energy (eV) secondary electrons to escape into the gas. In our detector configuration we are mostly interested in the low-energy secondary electrons which are stopped in the gas close to the convertor surface. These will start avalanches at the convertor surface. The centroid of such an avalanche precisely corresponds to the X-ray conversion point. On the other hand, long range primary electrons will produce broad, multi-electron, avalanches worsening the determination of the conversion point. The best localization expected would therefore be using convertors with an enhanced low energy secondary emission. As already discussed above, the best known candidate known is CsI.

The time resolution of our device has been investigated with a pulsed UV-source[17,24]. The time resolution is of the order of 0.35-4 ns (FWHM), for 20 to 1 emitted secondary electrons respectively. It should be noted that the full area of the detector was used for extracting the timing signals (64 cm^2). In real conditions this information could be measured on wires or small area pads, which would yield a better signal-to-noise ratio and thus improve the time resolution. Time resolutions of a few hundred ps (FWHM) are therefore expected with CsI, yielding on the average 17 secondary electrons per converted X-ray photon[10].

3. Application to Transition Radiation Detection

The traditional way of detecting TR photons (2-30 keV) is based on gas-filled proportional chambers[25-27]. TR photons, generated by Li or CH_2 (polypropylene) radiators, are converted in a high Z gas, usually Xenon mixed with CO_2. Photoelectrons from converted photons are detected by avalanche amplification. This technique provides high X-ray detection efficiency. However, the disadvantage of using a heavy gas mixture is that each passing particle deposits in the detector volume a large amount of highly fluctuating dE/dx ionization. The main effort of the TR detection is therefore in separating the charge deposited in the gas by TR photons from the dE/dx background. Since the TR photons are emitted along the particle's direction this task is difficult. The discrimination between the photoelectrons and the ionization electrons is usually done by measuring total charge and using a threshold, or by repeated measurements along the particle's trajectory using expensive FADC's (cluster counting). Statistical methods are used as well. δ-electron production along the particle's path complicates the TR detection by cluster counting.

As already mentioned above, traditional gaseous convertor-detectors are slow, with typical charge collection times of the order of 100 ns or more. "Straw" detectors were proposed as a replacement for traditional wire chambers. Their main advantage is in an improved time resolution, which is still of the order of several tens of ns[28]. The localization resolution is moderate. An interesting TR detector combining thin "straws" imbedded in a polyethylene foam radiator was recently tested[29]. Its time resolution is of the order of 30 ns.

TR detectors based on the proposed Secondary Emission technique are practically free of extended dE/dx background, due to the use of low-pressure electron multipliers. High TR conversion efficiency can be reached by carefully choosing the detector geometry. It is interesting to note that the effective atomic number of the proposed CsI convertor is 54, which is identical to that of Xenon. Therefore, for equal convertor "thickness" both the conversion efficiency and the yield of δ-rays is the same. This will be discussed further in Section 4.

As already discussed above, an excellent TR localization resolution is expected when using the tilted convertor geometry. It is of the order of 200 μm (FWHM) in one dimension and much better (200 $\mu \times \cos\theta$) in the other dimension. The expected time resolution is of the order of a few hundred ps (FWHM), which may be of prime importance for fast trigger purposes.

Two possible TRD geometries are shown in fig. 8. According to the experimental conditions the radiator can be either normal to the particle direction or parallel to the TR detector. The relevance of the radiator geometry will be discussed in the following paragraph.

The possible use of DME in the electron multiplier is of prime importance for low detector aging in high rate experiments.

4. Estimation of the TRD Efficiency.

It was established by Henke et al.[9] that in the case of X-ray radiation the maximum yield from a CsI photocathode is obtained in the range 3-6 keV, in consistency with the absorption cross-section. A considerable part of the Transition Radiation spectra of Lithium and Polypropylene falls into this energy range. Hence it is expected that efficient TR detectors with CsI convertors could be developed.

The spectrum of TR photons emitted from the radiator can be calculated using the standard *approximate formula*[30]:

$$\frac{dN_{TR}}{dE} = \frac{2\alpha\beta^2}{\pi E}\int \sin^3\varphi \left[\frac{1}{\kappa+\xi_1^2} - \frac{1}{\kappa+\xi_2^2}\right]^2 \times \left\{1+\exp(-\sigma_1) - \right.$$
$$\left. - 2\exp(-\sigma_1/2)\cos\Phi_1\right\} d\varphi \times \frac{1-\epsilon^{-N\sigma}}{1-\epsilon^{-\sigma}},$$

where $\beta = \frac{v}{c}$, γ the Lorenz' factor, $\kappa = \gamma^{-2} + \varphi^2$, $\alpha \cong \frac{1}{137}$, $\xi_i = \frac{\hbar\omega_{pl}^{(i)}}{E}$, $\omega_{pl}^{(i)}$ are the plasma frequencies in the media [radiator foil (i=1) and gas filling in the gap (i=2)].

The function Φ_1 is calculated from:

$$\Phi_1 = \frac{\hbar\omega_{pl}^{(1)} d_1}{2\hbar c\beta}\left[\kappa + \xi_1^2\right],$$

and

$$\sigma = \sigma_1 + \sigma_2 = \mu_1(E)d_1 + \mu_2(E)d_2$$

where μ_1 and μ_2, d_1 and d_2 are the linear absorption coefficients and the transverse dimensions of the radiator foil and gap respectively. The self absorption of the TR in the radiator stack is included, in an approximate way, through the last term in eq. 1, where N is the number of foils in the stack. In the case of an inclined incidence the d_i dimensions should be replaced by $d_i = d_i / \cos\theta$, (θ the angle of incidence, measured from the normal direction, as shown in fig. 8).

The total number of emitted TR photons per relativistic particle is obtained by integrating eq. (1):

$$N_{TR} = \int_{E_{th}}^{\infty} \frac{dN_{TR}}{dE} dE \,, \tag{2}$$

E_{th}, the threshold energy, is taken as 1 keV. N_{TR}=4–14 photons, depending on the characteristics of the radiator foils stack.

In figs. 9 and 10 the TR spectra are given from Li and CH_2 radiators for γ=4000 and for various incidence angles. The gap between the radiator foils is assumed to be filled with He. It is obvious that an inclined incidence shifts the spectrum towards the higher energy range and reduces the total TR photon yield, due to self-absorption. The effect is stronger in CH_2 than in Li. At θ=80° there is a structure in the spectrum, which is due to interference effects, and was also observed experimentally.

For a relativistic particle to be detected and identified with the present technique it is sufficient that one TR photon, out of the total number N_{TR}, is absorbed in the CsI photocathode. As follows from refs. 9 and 10, each X-ray photon absorbed in the CsI induces many secondary electrons, detected by the electron multiplier.

Using Monte Carlo simulations we have calculated the statistical distribution of the number of events in which one or more TR photons are absorbed in the CsI photocathode, for various incidence angles and CsI thicknesses[32]. From these data we deduce the relativistic particle detection probability, presented in fig. 11, for the geometry of fig. 8a.

The main problem in TRD is the competition from δ-rays induced by relativistic

particles traversing the detector's matter. In Xe-filled detectors the δ-ray background is of the order of 20% of the useful X-ray induced signal[27]. A priori, a CsI based detector should not have a higher δ-ray background than a Xe based detector of a comparable thickness, since the Z number is identical. On the contrary in CsI the self-absorption may help to reduce the contribution of low-energy δ-rays to the measurable signal. We have estimated the probability to have at least one δ-electron emitted from the CsI foil, using Möller's cross-section[31] and assuming a minimum energy of the δ-electron spectrum of 200 eV.

The estimated δ-ray background contribution is shown in fig. 11, assuming a Li radiator and γ=4000. This figure presents the detection probability for one or more TR photons and for δ-rays under the same geometrical arrangements (fig. 8a). Two cases are treated: a) the total number of TR photons is obtained from Eq. (2). b) the total number of TR photons is half that derived from Eq. (2). The latest (fig. 11b) is apparently a more realistic estimate, based on experimental data[27].

From fig. 11b it is evident that even if we assume a lower number of TR photons our detection efficiency is comparable to that of most Xe-based detectors, provided that we use the inclined geometry. A probability of about 60% to detect at least one TR photon is calculated for 60° and 400 nm thick CsI. However, for the same conditions the probability to detect δ-rays is considerably lower than in Xe detectors, and is of about 5% at 60°. From this figure it is also evident that the incidence angle of 60° is superior to 80°, both for X-ray detection efficiency and background rate. This is due to the lower self-absorption of the TR photons in the radiator foils (fig. 9).

In fig. 12 we present the same probabilities calculated for a geometry in which the radiator foils are normal to the incident beam (fig. 8b) but the CsI convertor foil is at an inclined angle to the particle beam (which is also the TR beam direction). This geometry is preferable since it avoids the hardening of the TR spectrum due to self-absorption in the radiator. In such an arrangement, according to fig. 12b, the best performance of the CsI convertor is obtained at 80°, having more than 90% probability to detect at least one X-ray with a 400 nm thick CsI convertor, and less than 15% of δ-ray

background, for a single TR detector element. Multifoil TR detector arrangements can be used in both cases to enhance the detection efficiency, as shown in fig. 8.

Similar calculations were done for CH_2 radiator foils. But due to the higher mean energy of the TR spectrum (fig. 10) the X-ray detection efficiencies with CsI are rather low, of the order of 25%[32].

These preliminary estimates will be further elaborated and followed by more accurate detector optimization calculations and experimental determination of secondary electrons induced by relativistic electrons. They will also take into account parameters such as gas composition and gas pressure in the gaps between the radiator foils[32].

Summary

A novel, ultrafast and high accuracy X-ray imaging method is proposed. It is based on the efficient emission, collection, multiplication and imaging of secondary electrons generated from solid convertors into multistage low-pressure gaseous multipliers.

This technique is suitable for a broad spectrum of applications in basic and applied research. Its main strength is in high localization accuracy (better than 200 μm FWHM) and subnanosecond timing at high X-ray flux.

The detection efficiency at a given X-ray energy is a function of the convertor material, thickness and geometry. CsI is a particularly interesting convertor material for soft X-rays. Tantalum convertors may be applied for imaging of high energy X- or gamma-ray photons. It is shown that DME, known for its low aging properties, can be used in the electron multiplier.

Detectors of this type may be efficiently employed for particle identification by Transition Radiation. Thin CsI convertors may very well replace thick Xenon gas detectors (Z=54 in both cases). The high localization accuracy, ultrafast response, low sensitivity to particle dE/dx background and the capability of operating at high counting rates make this detector a very competitive solution to particle identification in future colliders. The possibility of having an **ultrafast trigger** may be of prime importance in this field. Particle identification probabilities higher than 60% for an inclined radiator and 90% for a normal radiator are expected per single convertor foil-detector element,

according to our Monte Carlo simulations. The estimated δ-ray background is below 5% for an inclined radiator and 15% for a normal radiator. These values are lower than in Xe-filled TR detectors, the main reason being the self-absorption of the low energy ionization electrons in the solid as opposed to the gaseous medium. The dE/dx background from CsI convertors is presently being evaluated experimentally in our laboratory. Multiple TR detector elements may be coupled to each radiator, or to separate radiators, so as to increase particle identification probability.

It should be noted that for similar reasons particle identification via Synchrotron Radiation could make efficient use of this novel technique. Many other applications with high flux Synchrotron Radiation sources may greatly benefit from the ultrafast high accuracy, Secondary Emissions X-ray detection technique.

We are highly indebted to Dr. B. Dolgoshein for very stimulating discussions. We would like to thank Mr. I. Frumkin for his assistance in the localization measurements and Mrs. Y. Gil, Mr. J. Asher, Mr. M. Klin and Mr. L. Sapir for their valuable technical assistance. A.A. and A.G. would like to express their gratitude for the partial support of the Einstein Center for Theoretical Physics at the Weizmann Institute. S.M. would like to thank the Weizmann Institute staff for their hospitality during his stay. A.A. and V.E. were partially supported by the Center of Integration in Science of the Israel Ministry of Integration. This work was partially supported by the Minerva Foundation, Munich, Germany.

References

1. J.E. Bateman, Nucl. Instrum. Meth. **A273** (1988) 721 and references therein.
2. G. Charpak, CERN-EP/81-07, 1981. A contribution to the ESF-CNRS-EMBL Workshop on X-ray position sensitive detectors, Hamburg, 1980.
3. A. Breskin, G. Charpak, and J.C. Santiard, Nucl. Instrum. Meth. **195** (1982) 469.
4. U.W. Arndt, J. Appl. Cryst. **19** (1986) 145 and references therein.
5. A.T. Margarian, Publication EFI-516(3)-82 of Yerevan Inst. of Physics, 1981 (In Russian).
6. I. Dorion, U.Ruscav and A.P. Lilot, IEEE Trans. Nucl. Sci. **NS-34** (1987) 442.
7. A.F. Akkerman, V.A. Botvin, M. Ya. Grudskii, V.V. Smirnov, G.Ya. Chernov and M.V. Shilenkova, Phys. Stat. Sol. **B110** (1982) 285.
8. A.F. Akkerman, M.Ya. Grudskii, V.V. Smirnov, Secondary electron radiation emission from solids under the action of gamma-rays. Edited by Enezgevatomizdat-Moscow 1986 (in Russian).
9. B.L. Henke, J.P. Knower and K. Premasatue, J. Appl. Phys. **52** (1981) 1509.
10. S.A. Schwarz, J. Appl. Phys. **68**, (1990) 2382.
11. M.P. Kowalski, G.G. Fritz, R.G. Cruddace, A.E. Unzicker and M. Swanson, Appl. Opt. **25** (1986) 2440.
12. G.W. Fraser, Nucl. Instrum. Meth. **206** (1983) 265.
13. J.E. Bateman and R.J. Apsimon, Adv. Electron. Electron Phys., **52** (1979) 189.
14. D.G. Simons, G.W. Fraser, P.A.J. De Korte, J.F. Pearson and L. De Jong, Nucl. Instrum. Meth. **A261** (1987) 579.
15. V. Dangendorf, A. Breskin, R. Chechik and H. Schmidt-Böcking, Nucl. Instrum. Meth. **A289** (1990) 322.
16. V. Dangendorf, A. Breskin, R. Chechik and H. Schmidt-Böcking, Instrum. In Astronomy VII, Proc. SPIE 1235 (1990) 896.
17. V. Dangendorf, A. Breskin, R. Chechik and H. Schmidt-Böcking, Progress in Ultrafast CsI-Photocathode Gaseous Imaging Photomultipliers, Preprint WIS-

91/10/Apr.-PH. Nucl. Instrum. Methods, in press.

18. A. Breskin and R. Chechik, Nucl. Instrum. Methods **227** (1984) 24.
19. A. Breskin and R. Chechik, IEEE Trans. Nucl. Sci. **NA-32** (1985) 504.
20. A. Breskin and R. Chechik, Nucl. Instrum. Methods **264** (1988) 251.
21. S. Majewski, D.F. Anderson, P. Constanta-Fanourakis, B. Kross and G. Fanourakis, Nucl. Instrum. Methods **A264** (1988) 235.
22. A. Breskin, R. Chechik, G. Malamud and D. Sauvage, IEEE Trans. Nucl. Sci. **NS-36** (1989) 316.
23. G. Malamud, A. Breskin and R. Chechik, A systematic study of primary ionization cluster counting at low gas pressures. Preprint WIS-90/70/Nov -PH. Nucl. Instrum. Methods, in press.
24. A. Breskin, R. Chechik, V. Dangendorf, S. Majewski, G. Malamud, A. Pansky and D. Vartsky, New approaches to spectroscopy and imaging of ultrasoft-to-hard X-rays. Preprint WIS-90/55/Aug.-PH. Nucl. Instrum. Methods, in press.
25. G.B. Yodh, IEEE Trans. Nucl. Sci. **NS-31** (1984) 40 and references therein.
26. B. Dolgoshein, Nucl. Instrum. Methods **A252** (1986) 137.
27. B. Dolgoshein, The Transition Radiation Detectors, a review article, in preparation.
28. J. Shank, J. Beatty, T. Coan, A. Marin, S. Whitaker, R.J. Wilson and B. Zhou, Proc. Symp. on Particle ident. at high luminosity hadron colliders, FNAL, 1989, p. 399.
29. J.T. Shank et al., Test beam performance of a tracking TRD prototype, Preprint CERN-PPE/91-49 (1991) and B. Dolgoshein, Progress in Transition Radiation Detectors, these proceedings.
30. C.W. Fabjan and W. Struczinski, Phys. Lett. **57B** N5 (1975) 483.
31. C. Möller, Ann. Phys. **14** (1932) 531.
32. A. Akkerman, A. Breskin, R. Chechik and A. Gibrekhterman, An ultrafast Secondary Emission Transition Radiation Imaging Detector, in preparation.

Figure Captions

1. A schematic view of the Secondary Emission X-ray detector. A solid convertor is coupled to a low-pressure multistep secondary electron multiplier.
2. The amplification curve for single electrons in a single parallel gap: DME, p=20 Torr.
3. a) The pulse height distribution of secondary electrons induced by 8 keV photons in a 2000 Å thick CsI convertor. Isobutane, 18 Torr. The reduced electric field in the preamplification gap is 180 V/cm·Torr.

   b) The pulse height distribution of single electrons, photoproduced by UV photons under the same conditions as in a).
4. The pulse height distribution of single photoelectrons in the multistep detector of fig. 1. The total gain is of the order of 10^8. A saturation in amplification is clearly visible.

   a) DME, 20 Torr

   b) C_2H_6, 20 Torr
5. A tilted detector arrangement, enhancing the conversion efficiency (see text).
6. The conversion efficiency of X-ray photons in a 2000 Å thick CsI layer, for various incident angle values.
7. Two-dimensional image and its projection, obtained by irradiating the detector with 8 keV photons, at normal incidence, through a narrow slit. The slit width, projected at the convertor plane, is 70 μm. Isobutane at 8 Torr; CsI thickness 2000 Å.
8. Possible geometrical arrangements for TRD:

   a) The radiator foils and the TR detector are both tilted relative to the incident beam.

   b) The radiator foils are perpendicular to the beam; the TR detector modules are tilted.
9. Transition Radiation yield from a Li radiator, for various incidence angles. He at 1 atm between the radiator foils.

10. Transition Radiation yield from a polypropylene (CH_2) radiator for various incidence angles. He at 1 atm between the radiator foils.

11. Probability to detect one or more TR photons from a Li radiator converted in the CsI layer and the detection probability for δ-rays produced in the CsI, for various incidence angles in the geometrical arrangment of fig. 8a.

    a) The TR yield is calculated from eq. (2).

    b) The TR yield is taken to be half of that calculated by eq. (2).

12. Same as fig. 11 but for the geometrical arrangement of fig. 8b.

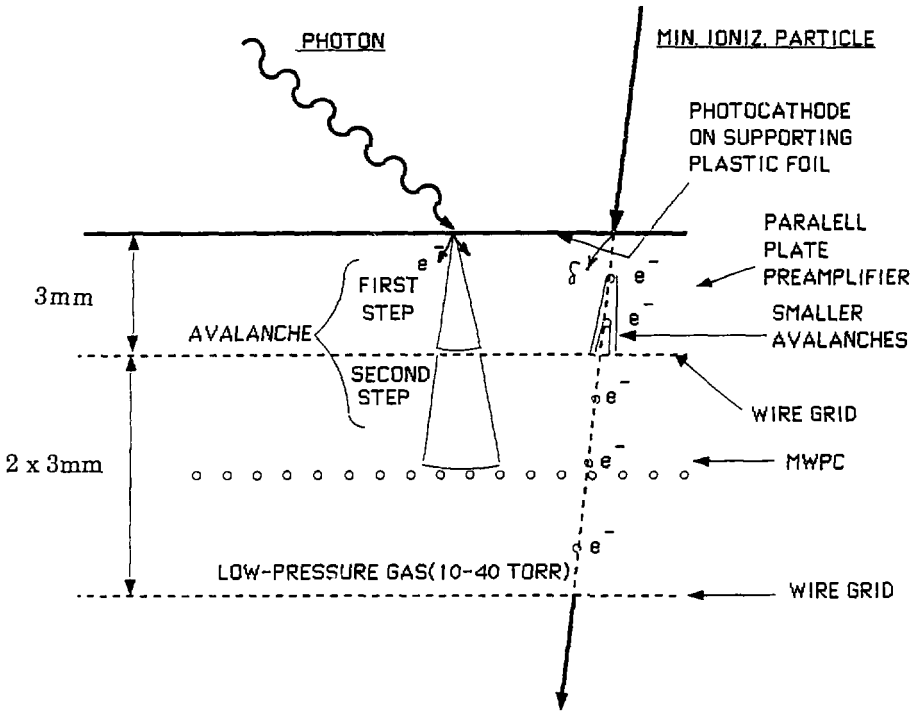
PHOTON
MIN. IONIZ. PARTICLE
PHOTOCATHODE
ON SUPPORTING
PLASTIC FOIL
PARALELL
PLATE
PREAMPLIFIER
SMALLER
AVALANCHES
3mm
AVALANCHE
FIRST
STEP
SECOND
STEP
WIRE GRID
2 x 3mm
MWPC
LOW-PRESSURE GAS(10-40 TORR)
WIRE GRID

Figure 1

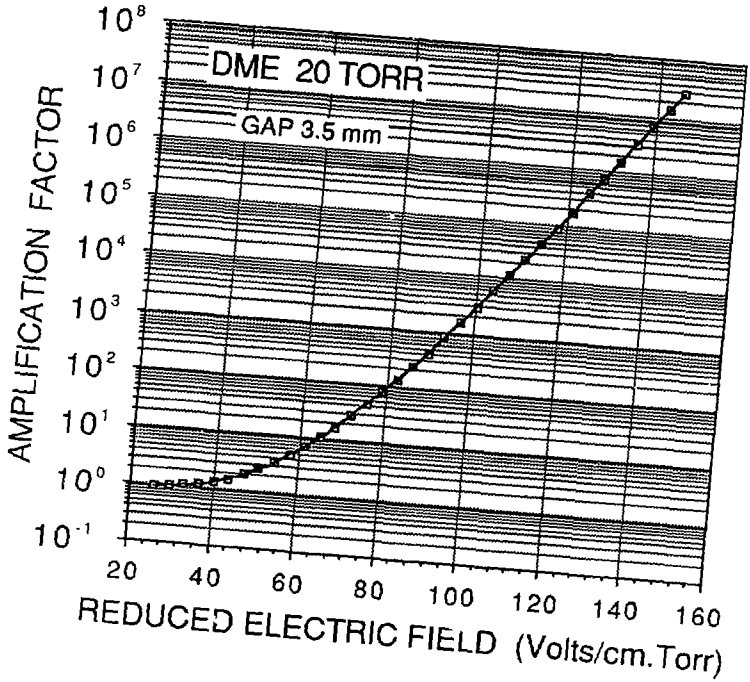
DME 20 TORR
GAP 3.5 mm
AMPLIFICATION FACTOR
10^8
10^7
10^6
10^5
10^4
10^3
10^2
10^1
10^0
10^{-1}
20
40
60
80
100
120
140
160
REDUCED ELECTRIC FIELD (Volts/cm.Torr)

Figure 2

a)

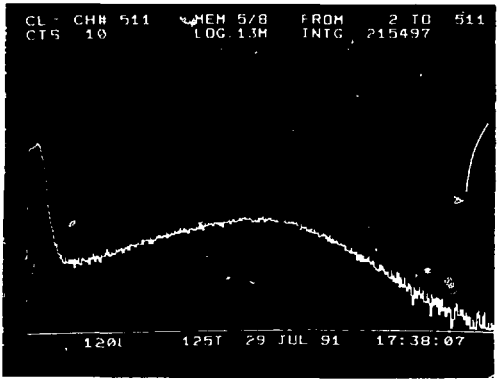
CL CH# 511 MEM 5/8 FROM 2 TO 511
CTS 10 LOG 1.3M INTG 215497
120I 125T 29 JUL 91 17:38:07

b)

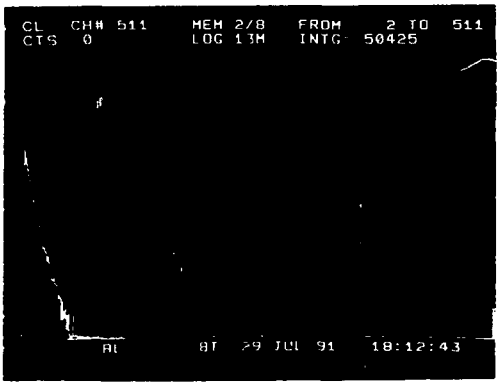
CL CH# 511 MEM 2/8 FROM 2 TO 511
CTS 0 LOG 1.3M INTG 50425
AL 8T 29 JUL 91 18:12:43

Figure 3

a)

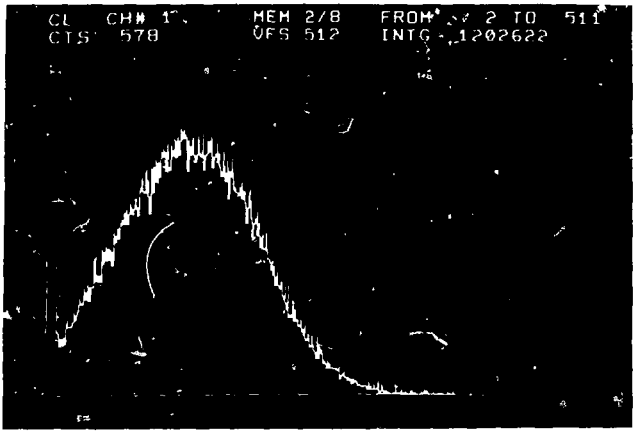
CL CH# 1
CTS 578
MEM 2/8
VFS 512
FROM 2 TO 511
INTG 1202622

b)

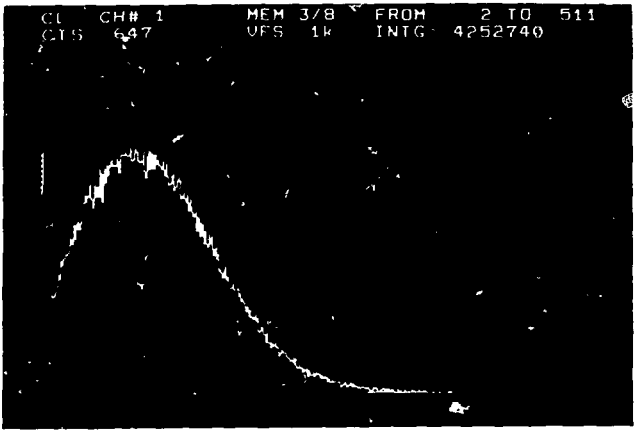
CL CH# 1
CTS 647
MEM 3/8
VFS 1k
FROM 2 TO 511
INTG 4252740

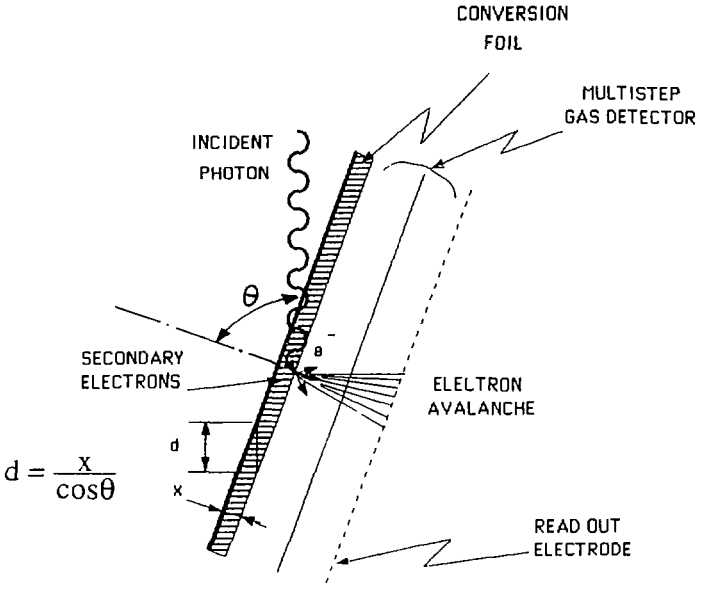
CONVERSION
FOIL
MULTISTEP
GAS DETECTOR
INCIDENT
PHOTON
θ
SECONDARY
ELECTRONS
ELELTRON
AVALANCHE
d
x
READ OUT
ELECTRODE
$d = \frac{x}{\cos\theta}$

Figure 5

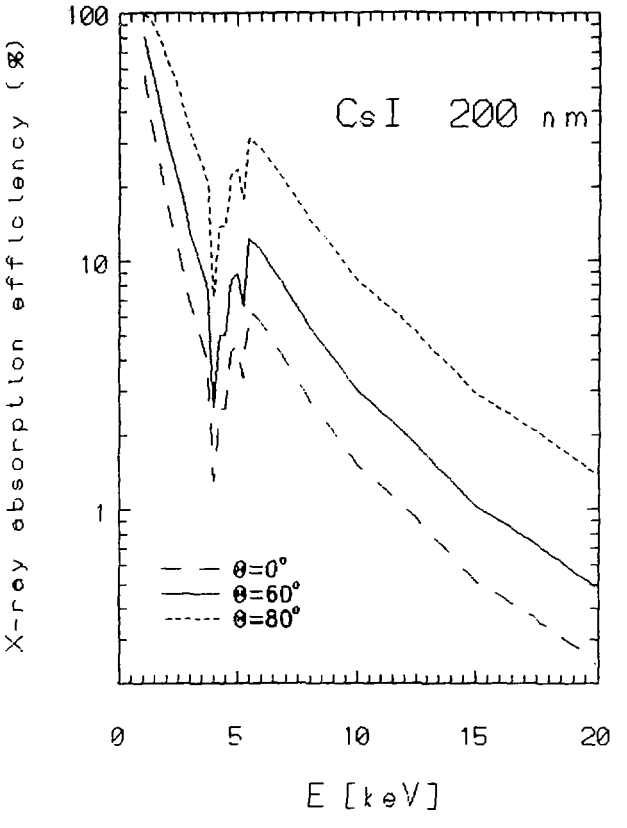
100
10
1
X-ray absorption efficiency (%)
CsI 200 nm
θ=0°
θ=60°
θ=80°
0
5
10
15
20
E [keV]

Figure 6

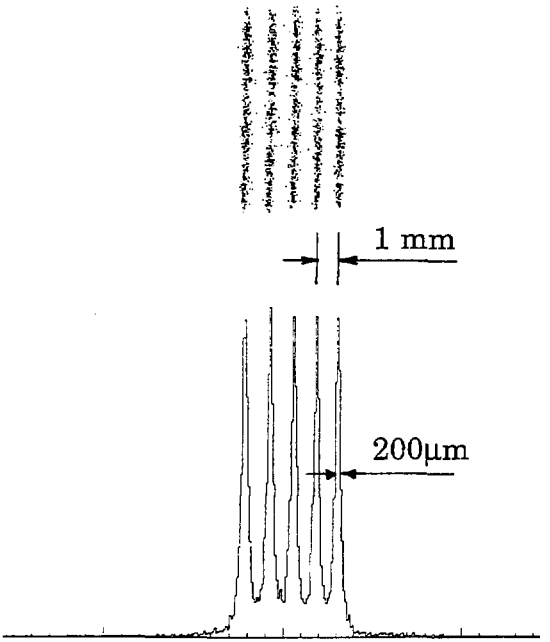

Figure 7

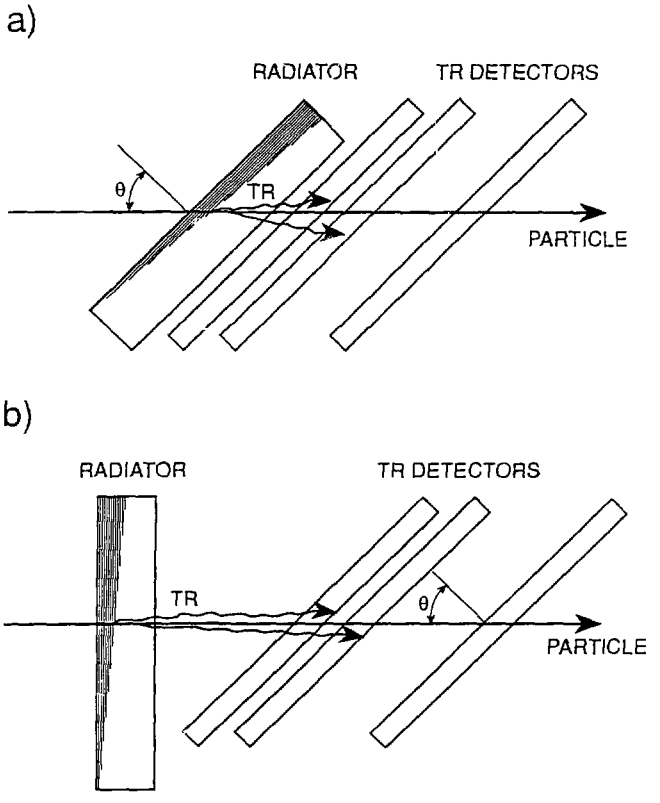
a)
RADIATOR
TR DETECTORS
θ
TR
PARTICLE
b)
RADIATOR
TR DETECTORS
TR
θ
PARTICLE

Figure 8

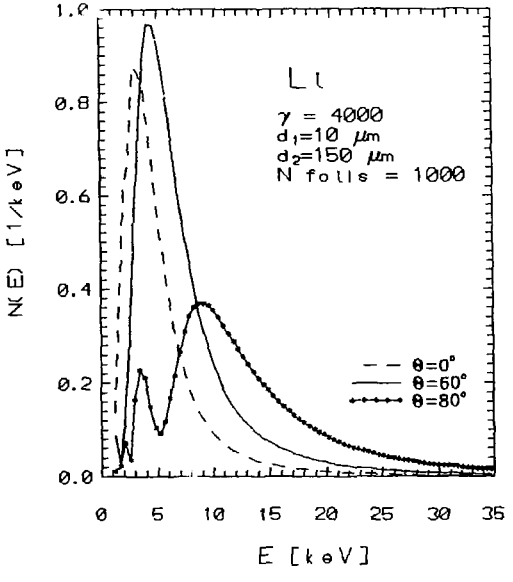

Figure 9

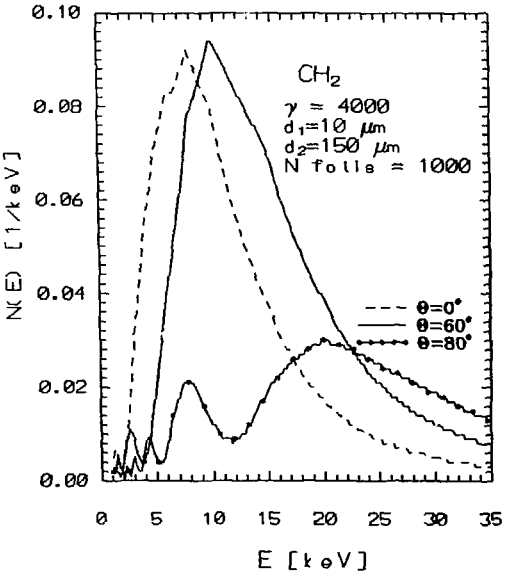

Figure 10

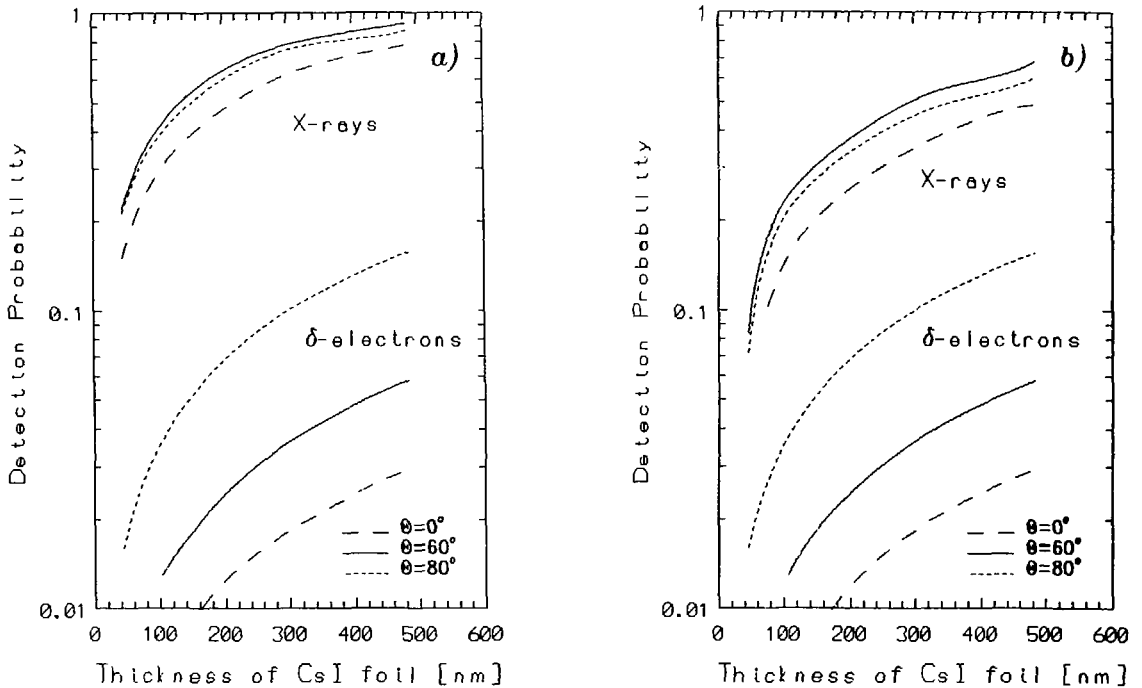
a)
b)
X-rays
δ-electrons
θ=0°
θ=60°
θ=80°
Detection Probability
Thickness of CsI foil [nm]
1
0.1
0.01
0
100
200
300
400
500
600

Figure 11

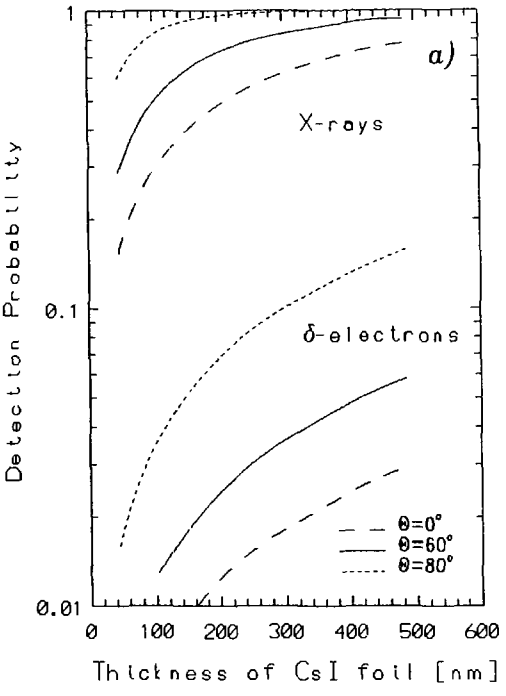
a)
X-rays
δ-electrons
θ=0°
θ=60°
θ=80°
Detection Probability
Thickness of CsI foil [nm]
1
0.1
0.01
0
100
200
300
400
500
600

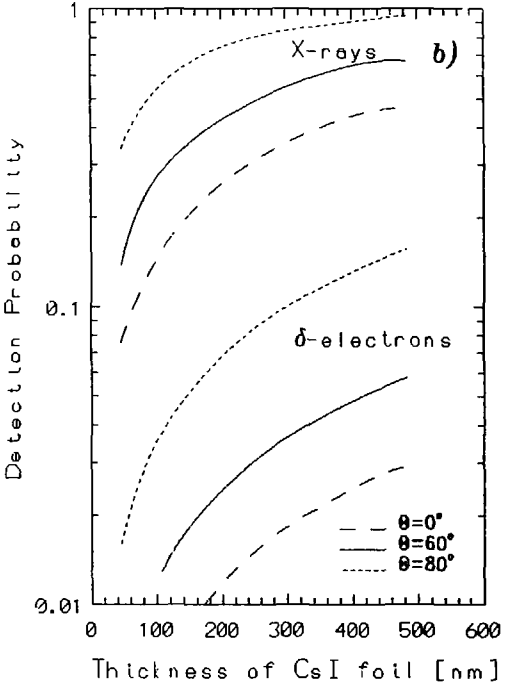
b)
X-rays
δ-electrons
θ=0°
θ=60°
θ=80°
Detection Probability
Thickness of CsI foil [nm]
1
0.1
0.01
0
100
200
300
400
500
600

Figure 12